

Post-Treatment-Free Dual-Interface Passivation via Facile 1D/3D Perovskite Heterojunction Construction

Ning Wei, Yanfeng Miao, Xingtao Wang, Zhixiao Qin, Xiaomin Liu, Haoran Chen, Haifei Wang, Yugang Liang, Shaowei Wang, Yixin Zhao,* and Yuetian Chen*



Cite This: *JACS Au* 2023, 3, 3324–3332



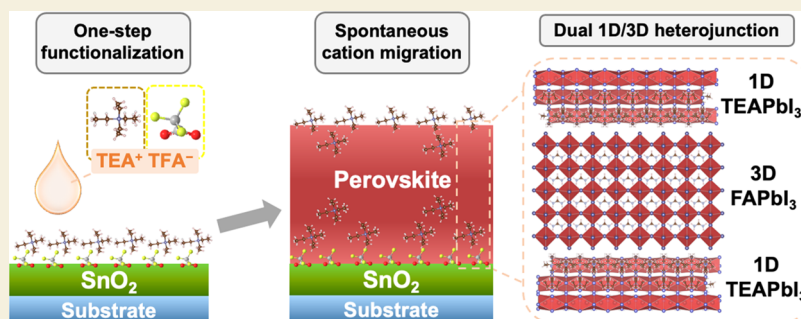
Read Online

ACCESS |

Metrics & More

Article Recommendations

Supporting Information



ABSTRACT: For achieving high-efficiency perovskite solar cells, it is almost always necessary to substantially passivate defects and protect the perovskite structure at its interfaces with charge transport layers. Such a modification generally involves the post-treatment of the deposited perovskite film by spin coating, which cannot meet the technical demands of scaling up the production of perovskite photovoltaics. In this work, we demonstrate one-step construction of buried and capped double 1D/3D heterojunctions without the need for any post-treatment, which is achieved through facile tetraethylammonium trifluoroacetate (TEATFA) prefunctionalization on the SnO_2 substrate. The functional TEATFA salt is first deposited onto the SnO_2 substrate and reacts on this buried interface. Once the FAPbI_3 perovskite precursor solution is dripped, a portion of the TEA^+ cations spontaneously diffuse to the top surface over film crystallization. The TEATFA-based water-resistant 1D/3D $\text{TEAPbI}_3/\text{FAPbI}_3$ heterojunctions at both the buried and capped interfaces lead to much better photovoltaic performance and higher operational stability. Since this approach saves the need for any postsynthesis passivation, its feasibility for the fabrication of large-area perovskite photovoltaics is also showcased. Compared to $\sim 15\%$ for a pristine $5\text{ cm} \times 5\text{ cm}$ FAPbI_3 mini-module without postsynthesis passivation, over 20% efficiency is achieved following the proposed route, demonstrating its great potential for larger-scale fabrication with fewer processing steps.

KEYWORDS: 1D/3D heterojunction, perovskite solar cell, metal oxide substrate functionalization, interface engineering, spontaneous ion diffusion

INTRODUCTION

Metal halide perovskites possess prominent photovoltaic properties with a certified power conversion efficiency (PCE) record of 26.1% achieved for single-junction cells.^{1–3} However, the relatively high density of trap states at the interfaces between the perovskite film and charge transport layers not only induces undesired nonradiative recombination but also impacts the long-term stability of the perovskite solar cells (PSCs).^{4–7} While black-phase formamidinium lead iodide (FAPbI_3) exhibits an ideal band gap and good thermal stability for high-efficiency PSCs,^{8–12} pristine $\alpha\text{-FAPbI}_3$ suffers from phase transition into the nonperovskite phase ($\delta\text{-FAPbI}_3$) under ambient conditions with the loss of photoactivity.^{13–15} Therefore, passivating defects at both interfaces,^{16–18} i.e., the exposed top surface that is open for post-treatment and the buried interface to the metal oxide substrate,^{19–23} could

comprehensively protect the perovskite structure for better photovoltaic performance and higher operational stability.

One-dimensional (1D) perovskite with superior environmental stability and decent optical properties is a good candidate to modify a three-dimensional (3D) perovskite film.^{24–27} In a 1D structure, linearly arranged $[\text{PbX}_6]^{4-}$ frameworks are wrapped by inactive organic cations and thus protected from moisture and oxygen ingression.^{28–32} From this

Received: August 12, 2023

Revised: October 31, 2023

Accepted: October 31, 2023

Published: November 21, 2023



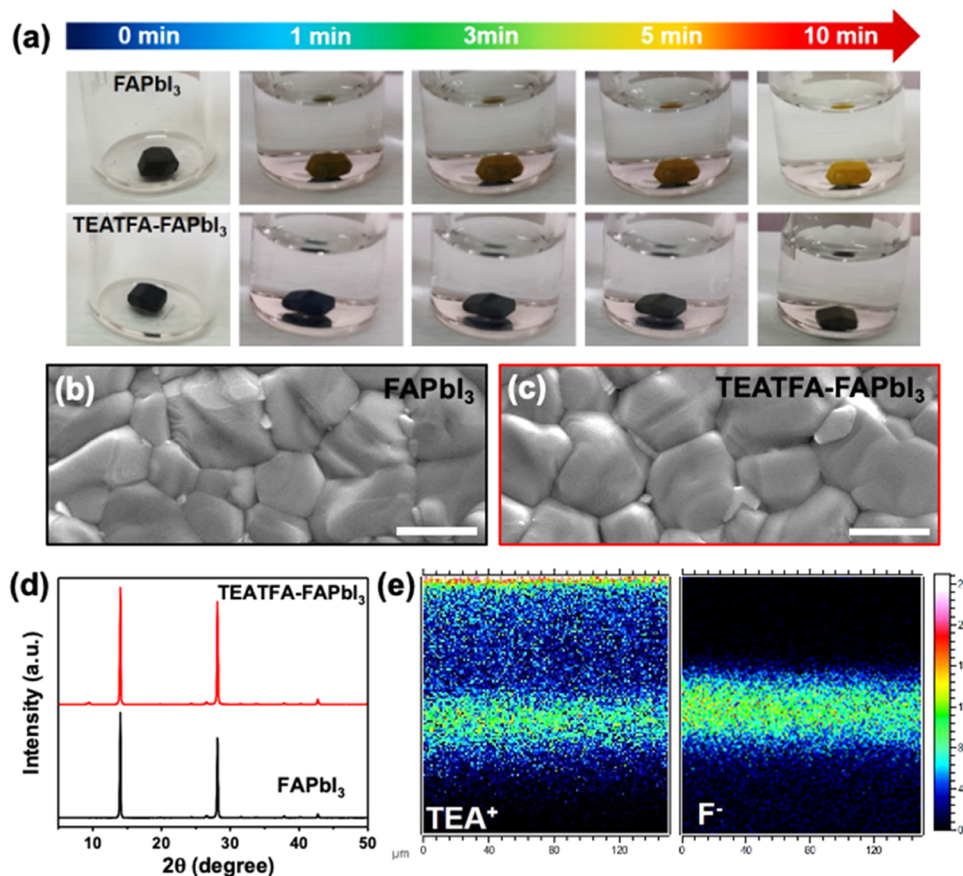


Figure 1. TEATFA-based structural modification to FAPbI₃ perovskite. (a) Photographs of FAPbI₃ single crystals without and with TEATFA treatment (TEATFA-FAPbI₃) that were immersed in ultrapure water over time. SEM images of (b) FAPbI₃ and (c) TEATFA-FAPbI₃ perovskite films. Scale bars represent 1 μm . (d) XRD patterns of the perovskite films. (e) Cross-sectional profiles from ToF-SIMS analysis showing the distribution of TEA⁺ and F⁻ signals across the TEATFA-FAPbI₃ perovskite film.

perspective, building a 1D/3D heterojunction on both interfaces can effectively passivate surficial defects and block the pathway of environmental invasion into the 3D bulk structure. Nonetheless, due to the technical difficulties of postsynthesis film deposition and dissolution, as well as some constraints on charge transport between perovskites of different dimensions, it is still challenging to achieve such dual-interfacial low-dimension engineering on perovskite solar cells with both improved structural stability and higher photovoltaic performance.^{33,34} Moreover, the postintroduction of a passivating agent is done through spin coating in most cases, which cannot meet the production demands of perovskite photovoltaics on a larger scale. All factors considered, developing comprehensive, feasible, and scalable dual-interfacial protection to the 3D perovskite layer using low-dimension perovskites but alleviating the hassle of post-treatment has rarely been explored.

Here in this work, we propose a facile but effective strategy for building a dual 1D/3D heterojunction at both buried and capped interfaces of the FAPbI₃ perovskite film by one-step substrate modification. The aforementioned technical challenges have been successfully overcome with only the buried interface to the SnO₂ charge transport layer functionalized by tetraethylammonium trifluoroacetate (TEATFA). A dual-interface 1D/3D perovskite heterojunction is spontaneously constructed via the migration and in situ reaction of the TEA⁺ cation with FAPbI₃ perovskite, where 1D perovskite gradient layers with superior water-resistant properties are formed at

both the buried interface and the top surface. The phase stability of the FAPbI₃ perovskite film is greatly enhanced with defect states on both interfaces passivated. Such a perovskite structure with well-suppressed defects endows the assembled solar cells with good operational stability and photovoltaic performance. While a low nonradiative recombination loss and a high PCE of 24.41% are achieved for the small-area cell, the 5 cm \times 5 cm mini-module with a larger area demonstrates over 20% efficiency without the need for any postsynthesis passivation steps, validating the effectiveness and feasibility of this heterojunction strategy, especially for large-scale flow-line production.

RESULTS AND DISCUSSION

TEATFA-Based Functionalization and In Situ Formation of Highly Stable 1D/3D Perovskite

1D TEAPbI₃ single crystals with good moisture stability were synthesized and are profiled in Figure S1. To explore the modification effect of TEATFA, FAPbI₃ single crystals with an average size of about 8 mm (Figure S2) were also synthesized and immersed in a TEATFA/isopropanol solution of 10 mg mL⁻¹ for minutes to obtain TEATFA-FAPbI₃. As shown in Figure 1a, when the pristine FAPbI₃ single crystal was soaked in ultrapure water, the perovskite surface rapidly became yellow over time, while the TEATFA-FAPbI₃ single crystal retained the original black phase (Figure S3) after being soaked for 10 min. It is suspected that this significant

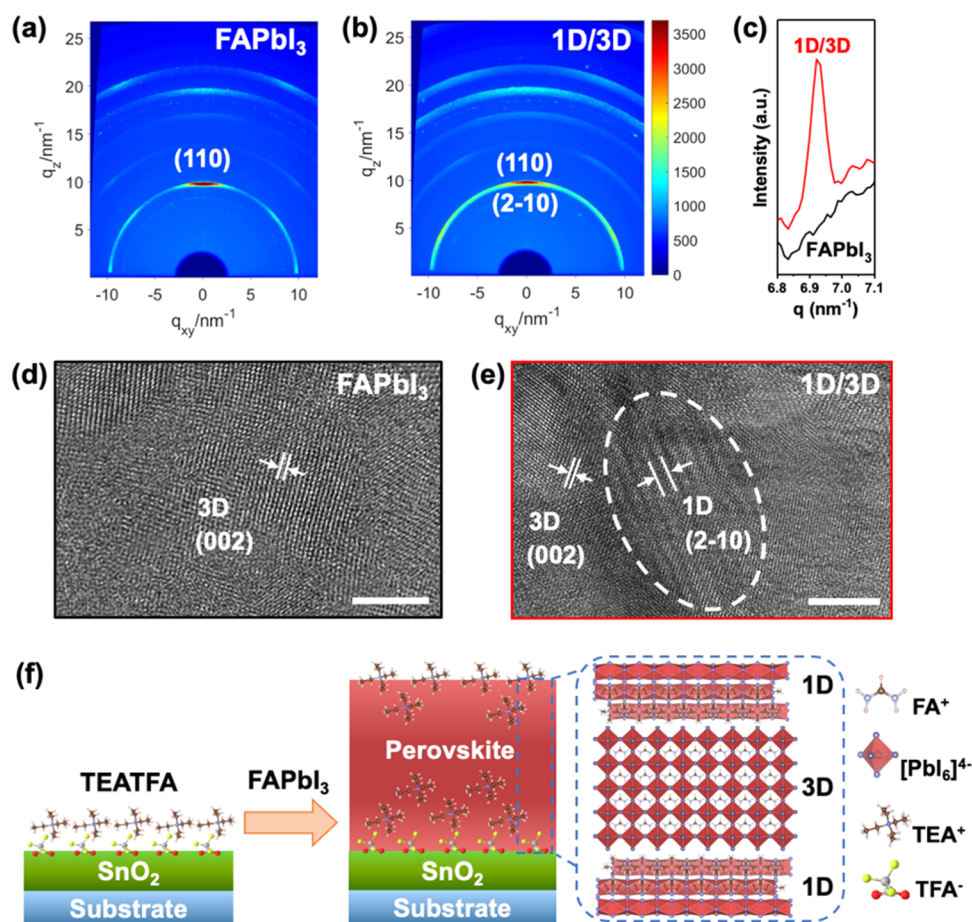


Figure 2. TEATFA-induced one-step 1D/3D dual-heterojunction formation. GIWAXS patterns of (a) FAPbI₃ and (b) 1D/3D perovskite films. (c) Integrated intensity profiles for FAPbI₃ and 1D/3D perovskite films. HRTEM images of (d) FAPbI₃ and (e) 1D/3D perovskite. Scale bars represent 5 nm. (f) Schematic illustration of the proposed sandwich-like 1D/3D dual-heterojunction structure.

improvement in moisture stability can be attributed to the transformation to 1D TEAPbI₃ perovskite of intrinsic water resistance. In order to investigate the mechanism of TEATFA-induced stability enhancement, as well as examine if such resistance could be retained in the form of a thin film, we soaked FAPbI₃ films separately in ultrapure water and a 10 mg mL⁻¹ TEATFA/water solution. As the crystalline and absorption profiles shown in Figure S4, the FAPbI₃ perovskite films degraded rapidly and turned into the PbI₂ phase after being soaked in water, while the films in the TEATFA/water solution still maintained the pristine features after soaking for 60 s. This result also suggested a TEA-induced 3D-to-1D perovskite transformation, as the FAPbI₃ perovskite films placed in TEATFA aqueous solution could react with the TEA⁺ cation to form a stable, protective layer of 1D TEAPbI₃ perovskite in situ.

To improve the stability at the buried interface of the FAPbI₃ film in an n-i-p solar cell architecture, TEATFA was predeposited on the SnO₂ substrate. The surface chemistry of the SnO₂ substrate was then studied by X-ray photoelectron spectroscopy (XPS). As the spectra shown in Figure S5, the emergence of the F 1s peak and the shift of the Sn 3d peak toward lower binding energy confirmed the anchoring of the TFA⁻ functional group on the SnO₂ surface. It is also expected that the TEA⁺ cation would react with the FAPbI₃ perovskite precursor to form the 1D/3D perovskite structure in situ. According to the top-view scanning electron microscopy

(SEM) images shown in Figure 1b,c, the modification to the buried interface has a negligible effect on the surface morphology of perovskite films. The band gap of bulk FAPbI₃ is also almost unchanged after the introduction of TEATFA, since the absorption edge is still at about 818 nm in the UV-vis spectra (Figure S6). XPS was also utilized to study the chemical states on the perovskite film surface. The slight shift of both Pb 4f and I 3d peaks in Figure S7 confirms the influence of the TEATFA-modified SnO₂ substrate on the chemical environment of the [PbI₆]⁴⁻ framework on the top surface of the FAPbI₃ film. Nonetheless, a small diffraction peak at 9.35° is observed in the XRD patterns of the TEATFA-FAPbI₃ sample (Figure 1d), which suggests the formation of 1D TEAPbI₃ perovskite on the surface. Time-of-flight secondary ion mass spectrometry (ToF-SIMS) was applied to reveal the distribution of critical ions in the perovskite film. As the cross-sectional and 3D mapping results shown in Figures 1e and S8, while the F⁻ from TFA⁻ only accumulated proximate to the buried interface to SnO₂, the TEA⁺ cation enriched at both the buried interface and the top surface of the TEATFA-FAPbI₃ perovskite film, exhibiting a unique spontaneously formed dual-gradient sandwich-like distribution. The ToF-SIMS depth profiles of several cations across this film (Figure S9) also confirm such a distributional trend of TEA⁺. Since the signal of TEA⁺ here is most likely related to the formation of a 1D TEAPbI₃ perovskite structure, it is speculated that a 1D/3D TEAPbI₃/FAPbI₃ heterojunction

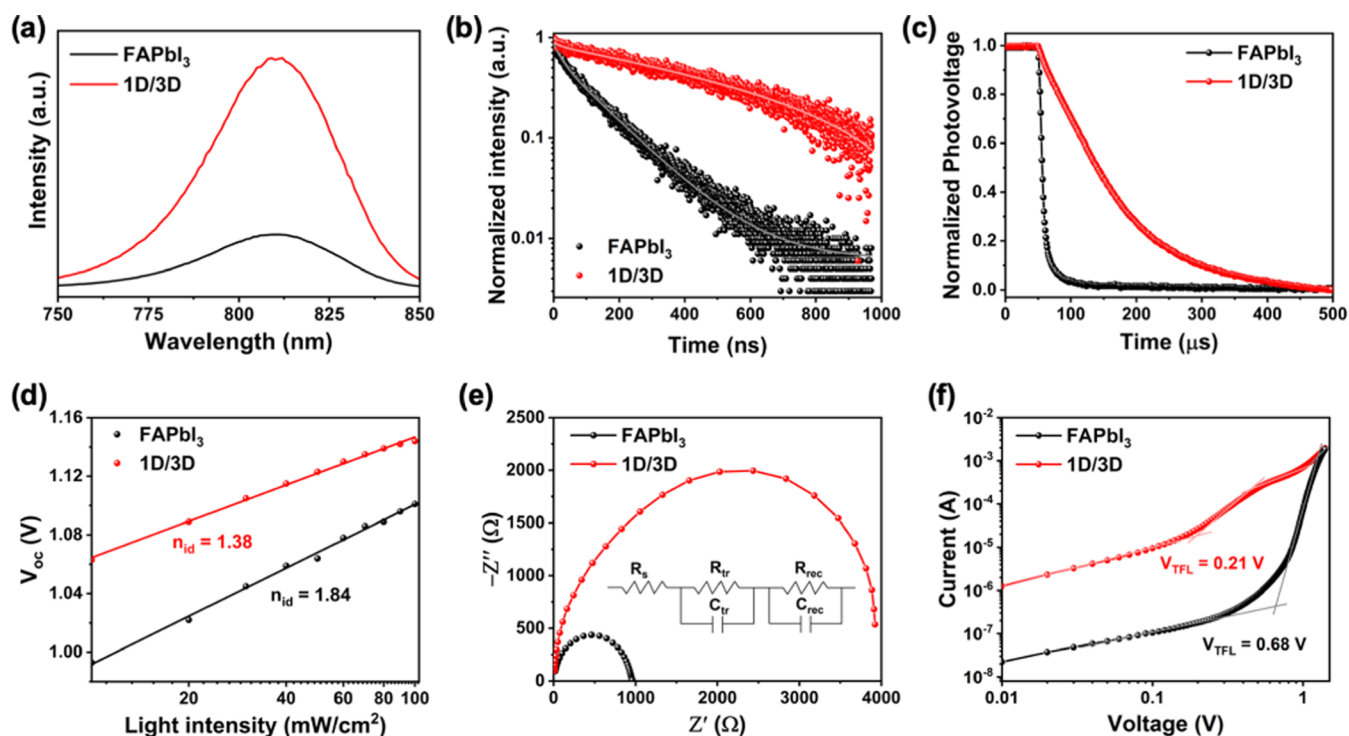


Figure 3. Defect passivation enabled by the 1D/3D dual-heterojunction structure. (a) PL emission spectra and (b) TRPL decay curves of FAPbI₃ and 1D/3D perovskite films deposited on the SnO₂ substrate and measured from the perovskite side. (c) TPV curves, (d) the relationship between V_{oc} and light intensity, and (e) the Nyquist plots of the FAPbI₃ and 1D/3D PSCs, inset: the equivalent circuit. (f) Current–voltage curves for the electron-only devices from SCLC measurements.

has formed at both interfaces of the film, and the TEATFA–FAPbI₃ perovskite sample is denoted 1D/3D from here on in this study.

One-Step Construction of the Dual-Interface 1D/3D TEAPbI₃/FAPbI₃ Heterojunction

To further explore the crystalline profiles of the perovskite films, the technique of synchrotron-based grazing incidence wide-angle X-ray scattering (GIWAXS) was employed. As the GIWAXS analysis result compared in Figure 2a–c, a new diffraction spot emerges at about $q_z = 6.9 \text{ nm}^{-1}$ for the 1D/3D film, which can be ascribed to the (2–10) plane of 1D TEAPbI₃ perovskite.³⁰ High-resolution transmission electron microscopy (HRTEM) images were acquired to study the effect of TEATFA on the microstructure of 3D perovskite films. As shown in Figure 2d,e, the fringe spacing of 0.936 nm correlates well to the (2–10) lattice plane of the 1D TEAPbI₃ perovskite.

Based on these characterization results, a scheme is illustrated (Figure 2f) to describe the proposed heterojunction engineering process. Generally speaking, the SnO₂ substrate was first functionalized with TEATFA, and then when a FAPbI₃ film was deposited and annealed on top, the TEA⁺ cation would diffuse to either the top surface or the buried interface with not much staying in the bulk perovskite structure. This diffusion preference of TEA⁺ toward the interface can be attributed to its structural and chemical properties.³⁰ The slightly larger size and hydrophobicity of this quaternary alkylammonium cation deem its proximity to the interface instead of residing inside the 3D bulk structure,³⁵ which resembles the function of a surfactant in nanoparticle synthesis.³⁶ In detail, during the deposition process of the FAPbI₃ film, the TEA⁺ cation and the TFA[−] anion on the

SnO₂ substrate would interact with the components in the perovskite precursor solution. Then, over the nucleation and growth stages, the steric constraint posed by the [PbI₆]^{4−} octahedral framework on TEA⁺ cations, as well as the tendency to form low-dimensional structures, pushes them to the top surface or at the buried interface. Following this unique distribution pattern and the reaction between TEA⁺ with native FAPbI₃, 1D TEAPbI₃ perovskite is formed in situ at not only the interface to the treated SnO₂ layer but also the top surface of the perovskite film. A dual-gradient sandwich-like protective structure was thus built as 1D/3D TEAPbI₃/FAPbI₃ perovskite heterojunctions on both interfaces, which ensures comprehensive protection and passivation. Meanwhile, owing to the stronger affinity between F and Sn,³⁷ the TFA[−] anion would maintain status quo over the annealing process and not diffuse to the top surface of the FAPbI₃ film, yielding the difference in distribution between the functional cation and anion. It has been reported that TEA⁺ is more inclined to react with defected Pb and I sites,³⁸ where binding energy is more negative than the defect-less sites. Considering the generally higher defect density of the film interfaces, the TEA⁺ cation would spontaneously migrate to those positions for defect passivation and in situ phase transformation to 1D TEAPbI₃ of intrinsically higher stability.

Effective Defect Passivation and Stability Enhancement by Dual-Interface 1D/3D Heterojunction Engineering

The overall stability improvement from such a dual-interface 1D/3D heterojunction on the perovskite thin film was then investigated. As the results shown in Figure S10, when exposed to the ambient atmosphere at room temperature for 36 h, the FAPbI₃ films severely degraded, while the 1D/3D films mostly retained the material's pristine properties. Therefore, the TEA-

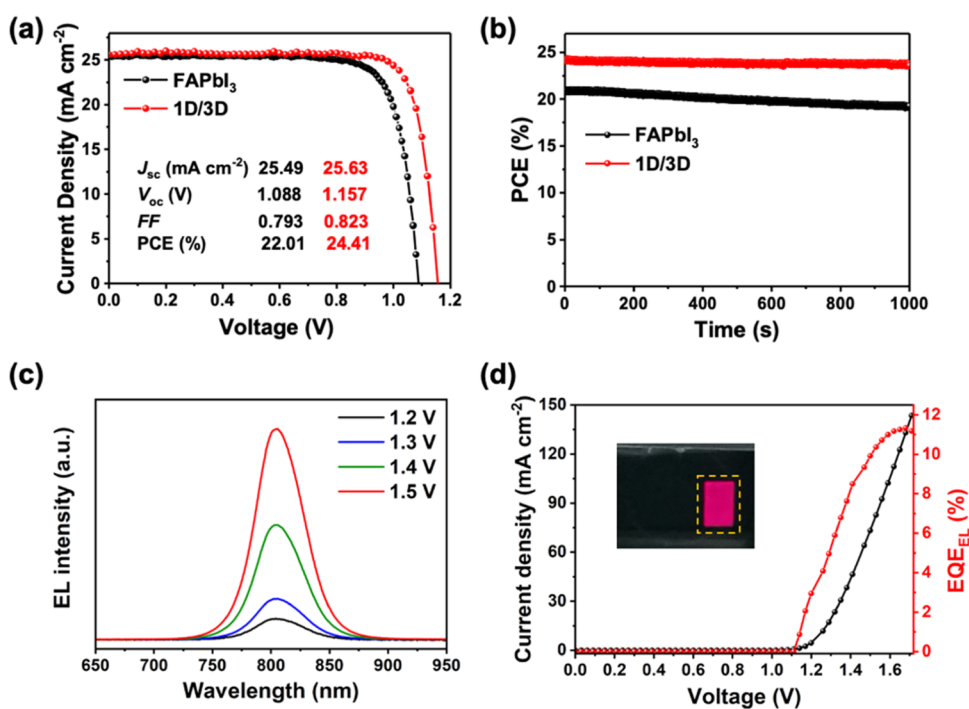


Figure 4. Photovoltaic and optoelectronic performance of solar cells based on the dual 1D/3D heterojunction perovskite. (a) Current density–voltage curves of the champion devices with an area of 0.085 cm^2 under simulated AM 1.5G illumination of 100 mW cm^{-2} measured in reverse scan, and (b) the stable output at the maximum power point for FAPbI₃ and 1D/3D PSCs. (c) EL spectra and (d) EQE_{EL} and current density of the 1D/3D device under varied bias voltages. Inset: photograph of the luminescence from the 1D/3D device.

induced in situ 1D perovskite formation and the consequently constructed 1D/3D perovskite heterojunction, in the form of either a thin film or a single crystal, has provided the material with good protection against environmental interference, especially moisture ingress.

The construction of the 1D/3D dual-interface heterojunction may also favorably tune the excited-state properties of the FAPbI₃ films. To investigate such impact, steady-state photoluminescence (PL) and time-resolved photoluminescence (TRPL) spectroscopy techniques were utilized. As shown in Figure 3a, the PL intensity for the 1D/3D perovskite film is much higher than that of the pristine FAPbI₃ film, indicating reduced defect density in the 1D/3D perovskite film. The TRPL decay curves in Figure 3b fit well to the biexponential functions (Table S1), which consist of a fast decay (τ_1) and a slow decay (τ_2).³⁹ Compared with FAPbI₃ (128.97 ns), the average decay lifetime (τ_{ave}) for 1D/3D perovskite (1012.37 ns) obviously increased, which demonstrates the decrease in nonradiative recombination by trap passivation after the introduction of 1D perovskite.

Based on the characterization of the 1D/3D perovskite film on the SnO₂ substrate, it is expected that with enhanced structural stability and reduced defect density, the fabricated solar cells would exhibit improved photovoltaic performance. To this end, n–i–p solar cells with a typical planar configuration of FTO/TiO₂/SnO₂/perovskite/spiro-OMeTAD/Au were fabricated. Figure S11 shows the cross-sectional SEM images for these representative cells based on FAPbI₃ with and without the introduction of a 1D perovskite. We used transient photovoltage decay (TPV) and transient photocurrent decay (TPC) measurements to investigate the charge transport properties of 1D/3D PSCs. As shown in Figure 3c, the 1D/3D PSCs show a longer photovoltage decay lifetime (126.6 μs) than the FAPbI₃ device (11.0 μs), which indicates

reduced undesired charge-carrier recombination. Meanwhile, a faster response on the photocurrent decay (Figure S12) is exhibited by the 1D/3D PSCs (5.16 μs) than the FAPbI₃ device (8.63 μs), illustrating slightly faster charge transport or collection and fewer trapping effects with the buildup of the dual-heterojunction structure. This observation on carrier dynamics corroborates with some previous studies on the positive influence of the 1D TEAPbI₃ ultrathin layer when capped on a 3D perovskite film.^{30,35} The recombination state in PSCs can also be demonstrated by the ideality factor (n_{id}), which is extracted from analyzing the relationship between the open-circuit voltage (V_{oc}) and light intensity.⁴⁰ As shown in Figure 3d, the n_{id} value decreased from 1.84 to 1.38 for 1D/3D PSCs, suggesting that the charge-carrier recombination has been effectively suppressed. Electrochemical impedance spectroscopy (EIS) was used to further evaluate the charge recombination process in photovoltaic devices after the introduction of 1D perovskite. As the Nyquist plots shown in Figure 3e and the values extracted in Table S2, the 1D/3D device exhibited higher charge recombination resistance (R_{rec}), corroborating the results on fewer unfavored carrier recombination.⁴¹

To quantify the trap density in the obtained films, space-charge-limited current (SCLC) measurements for electron-only devices were conducted (Figure 3f). The trap density (N_{traps}) was determined by the following formula⁴²

$$N_{traps} = \frac{2\epsilon\epsilon_0 V_{TFL}}{eL^2} \quad (1)$$

where ϵ is the relative dielectric constant of FAPbI₃,⁴³ ϵ_0 is the vacuum permittivity, V_{TFL} is the trap-filled limit voltage, e is the elementary charge, and L is the thickness of the perovskite film. The calculated N_{traps} value significantly decreases from $1.87 \times$

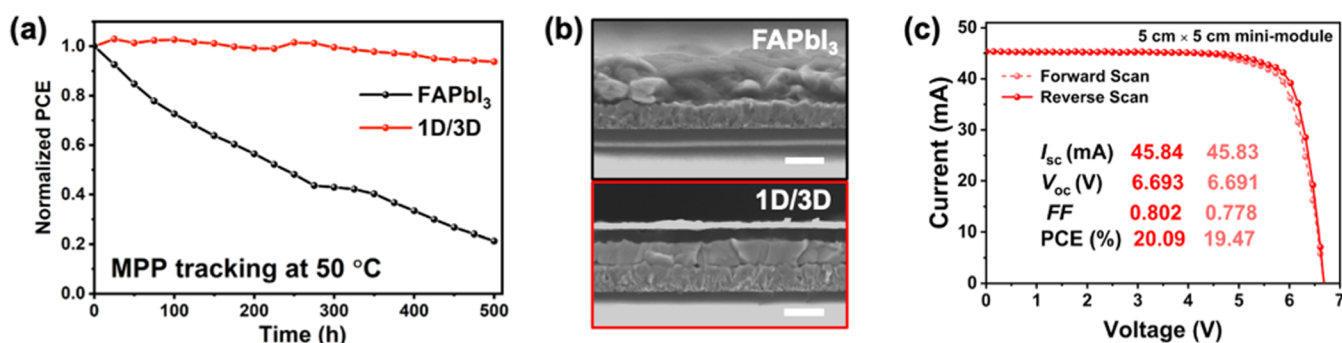


Figure 5. Stability of the small-area device and scalability to the large-area mini-module based on the dual 1D/3D heterojunction perovskite. (a) MPP tracking on the FAPbI₃ and 1D/3D PSCs under continuous light illumination at 50 °C in nitrogen. (b) Cross-sectional SEM images for the aged FAPbI₃ and 1D/3D devices after the MPP tracking. Scale bars represent 1 μ m. (c) Current–voltage curves of the 5 cm \times 5 cm 1D/3D perovskite mini-module in both forward and reverse scans.

10^{16} to 5.78×10^{15} cm⁻³ after the construction of the sandwich-like structure on the FAPbI₃ film, which further confirms the passivation effect of 1D perovskite. It is also important to prove that the fabrication of dual 1D/3D heterojunctions on both interfaces could passivate the defects more effectively than those with only one interface modified. To obtain such a sample, tetraethylammonium iodide (TEAI) was deposited on the annealed FAPbI₃ film as a post-treatment agent, where 1D perovskite was only introduced on the top surface with the sample denoted as 3D–1D. As compared in Figure S13, the single-interface-modified device presented a much higher N_{traps} value than the 1D/3D device, confirming the more effectual defect passivation of the proposed dual-interfacial method.

Good Performance and Scaling-Up Feasibility of Perovskite Photovoltaics Based on the 1D/3D Heterojunction

As shown in Figure 4a, the FAPbI₃-based device exhibited a PCE of 22.01% with a short-circuit current density (J_{sc}) of 25.49 mA cm⁻², a V_{oc} of 1.088 V, and a fill factor (FF) of 0.793. After the construction of the sandwich-like structure, the champion 1D/3D device exhibited a much higher PCE of 24.41% with a J_{sc} of 25.63 mA cm⁻², a V_{oc} of 1.157 V, and an FF of 0.823. Moreover, the 1D/3D devices showed higher reproducibility than the FAPbI₃ devices (Figure S14). In comparison to the post-treated, single-interface-modified 3D–1D devices, the dual 1D/3D devices also exhibited generally higher efficiency (Figure S15). Furthermore, the champion 1D/3D device showed a more stable output at the maximum power point (MPP) as compared in Figure 4b. Figure S16 displays the external quantum efficiency (EQE) spectra and the integrated photocurrent density of the PSCs. The EQE value of 1D/3D PSCs is >90% for wavelengths between 415 and 710 nm. The integrated J_{sc} calculated from EQE reached 24.77 mA cm⁻² for the 1D/3D PSCs compared with 24.39 mA cm⁻² of the FAPbI₃ device.

The data above have demonstrated that the construction of the dual 1D/3D heterojunction could effectively passivate defects and suppress the nonradiative recombination in PSCs, thus achieving enhanced photovoltaic performance. To further illustrate the contribution of the reduced nonradiative recombination to low voltage loss, electroluminescence (EL) and electroluminescence quantum efficiency (EQE_{EL}) evaluations were conducted. As compared between Figures 4c and S17, the intensity of the EL emission spectra of the 1D/3D

PSC is relatively higher than that of the FAPbI₃ device under corresponding bias voltages. The EL emission of 1D/3D PSC was detected even under a bias voltage as low as 1.08 V, suggesting low leakage current, low energy loss, and low nonradiative recombination.⁹ As shown in Figures 4d and S18, compared to 1.2% of the FAPbI₃ device, the 1D/3D device presents a higher EQE_{EL} of 6.3% for an injection current density of 25.5 mA cm⁻² that corresponds to J_{sc} . The nonradiative recombination loss can be calculated by the following formula⁴⁴

$$q\Delta V_{OC}^{non-rad} = -kT \ln(EQE_{EL}) \quad (2)$$

where k is the Boltzmann constant and T is the temperature. Therefore, a low nonradiative recombination loss of 71 mV was achieved for the 1D/3D perovskite solar cell, which was greatly reduced from 114 mV of the FAPbI₃ device.

As the stability of FAPbI₃ films remarkably improved with the passivation of stable 1D perovskite, we further evaluated the operational stability of the fabricated solar cells under MPP tracking with continuous illumination from a white LED lamp in a nitrogen atmosphere at 50 °C. The 1D/3D device maintained over 94% of its initial efficiency after 500 h, while the efficiency of the FAPbI₃ device decreased to about 20% of the original value (Figure 5a). According to the cross-sectional SEM images in Figure 5b, after the aging from the MPP test, the 1D/3D device still exhibits a layered profile, while the structure of the FAPbI₃ device has severely degraded. The 1D/3D device also showed promising enhancement in stability against moisture ingress (Figure S19), where 95% of the original efficiency was well retained after 480 h of monitoring under 85% RH at room temperature with simple device encapsulation. Therefore, the introduction of a 1D perovskite via dual-heterojunction engineering can effectively enhance the operational stability of FAPbI₃-based PSCs against environmental stresses.

For the industrial promotion of perovskite photovoltaics, it is crucial to simplify the processing steps. In this context, the ease of one-step substrate functionalization and spontaneous ion diffusion for dual-interface modification in the proposed approach could greatly benefit large-area fabrication. To demonstrate the scalability of our strategy, 5 cm \times 5 cm perovskite solar mini-modules (PSMs) consisting of six subcells with an aperture area of 12.25 cm² were fabricated. A certified efficiency of 20.09% (report from Shanghai Institute of Microsystem and Information Technology, SIMIT, attached in Figure S20) was achieved as the current–voltage curves and

the photovoltaic parameters from both forward and reverse scans shown in Figure 5c. The stable output of the PSM at the maximum power point is also evaluated, as shown in Figure S21. The good performance of the obtained PSMs proved that this strategy could tactfully circumvent the previously mentioned conventional technical difficulties of film damage or dissolution during post-treatment, which would be promising for the quality control and standardized flow-line production of large-area perovskite photovoltaics.

CONCLUSIONS

In summary, we have developed and constructed a highly stable perovskite structure with dual 1D/3D heterojunctions spontaneously formed at both buried and capped interfaces by a simple one-step SnO_2 substrate modification. The introduced 1D TEAPbI₃ perovskite could greatly improve the stability of the 3D structure against various external factors, especially humidity, which is crucial for the further promotion of high-efficiency FAPbI₃-based photovoltaics. Based on such all-round protection, this model could effectively passivate defects, suppress harmful nonradiative recombination, and improve the stability of thin films and the corresponding devices. As a result, the 1D/3D solar cell with the perovskite layer modified at both interfaces achieved a high PCE and a low nonradiative recombination loss. More importantly, this strategy without the need for any postsynthesis passivation can be well extended to the fabrication of 5 cm × 5 cm large-area perovskite photovoltaics with over 20% efficiency. This work provides a facile and effective strategy of in situ dual-interfacial heterojunction engineering that can circumvent the technical challenges brought by the conventional post-treatment, which can serve as a promising route toward preparing efficient and stable perovskite-based optoelectronics, especially for standardized production in larger scales.

MATERIALS AND METHODS

Single Crystal Synthesis

To grow FAPbI₃ single crystals, formamidinium iodide (FAI, 99.5%) and lead iodide (PbI₂, 99.999%) with a 1:1 molar ratio were dissolved in a mixed solvent of γ -butyrolactone (GBL) and formic acid (99%) in a 50:1 volume ratio at room temperature. The homogeneous precursor solution was then placed in an oil bath and slowly heated to 120 °C at 10 °C per hour. After the solution was kept at 120 °C overnight, FAPbI₃ single crystals were obtained. To grow TEAPbI₃ single crystals, 0.2 mmol of tetraethylammonium trifluoroacetate (TEATFA) and 0.2 mmol of PbI₂ were dissolved in the mixed solution of 3 mL of hydriodic acid (HI, 55.0–58.0% aqueous solution) and 0.2 mL of H₃PO₂ at 110 °C. The solution was then gradually cooled to room temperature at 5 °C per hour, and the TEAPbI₃ single crystals were seeded out.

Device Fabrication

A compact TiO₂ layer with a thickness of about 15 nm was deposited on patterned FTO (TEC-7) by atomic layer deposition using the precursor of tetrakis(dimethylamino) titanium. SnO_2 was deposited on the TiO₂/FTO substrate by spin-coating the tin(IV) oxide colloid precursor (15% in H₂O colloidal dispersion) in ammonium hydroxide at 3000 rpm for 30 s and then annealed at 180 °C for 0.5 h in air. A 1 mg mL⁻¹ TEATFA/ethanol solution was then spin-coated on the SnO_2 /TiO₂/FTO substrate at 3000 rpm for 30 s and annealed at 60 °C for 10 min in air. A 1.5 M FAPbI₃ precursor solution was prepared by dissolving FAPbI₃ single crystals and methylamine hydrochloride (MACl) with a molar ratio of 1:0.35 in the mixed solvent of *N,N*-dimethylformamide (DMF, anhydrous, 99.8%) and dimethyl sulfoxide (DMSO, anhydrous, 99.8%) in a 9:1 volume ratio. The perovskite

film was deposited on the SnO_2 /TiO₂/FTO substrate with or without TEATFA treatment by spin-coating the prepared precursor at a speed of 5000 rpm for 20 s. 1 mL of diethyl ether (DE) was dripped on the spinning substrate on the countdown of 15 s. The obtained perovskite film was then annealed at 150 °C for 10 min and 100 °C for 10 min. A hole-transport material (HTM) solution containing 0.1 M spiro-OMeTAD, 0.035 M bis(trifluoromethane)sulfonimide lithium salt (Li-TFSi), and 0.12 M 4-*tert*-butylpyridine (tBP) in chlorobenzene (CB, anhydrous, 99%) was then spin-coated onto the perovskite film at 4000 rpm for 20 s. Finally, a Au contact layer with a thickness of 100 nm was deposited by thermal evaporation. For the fabrication of 5 cm × 5 cm perovskite solar mini-modules, the FTO substrate was first etched by a 532 nm nanosecond laser scribe (GPLe-SLM50, Glory Photonics Technology Co., Ltd.) to form P1 lines. Then, P2 lines were etched after the coating of HTL, and P3 lines were etched after electrode deposition. The widths of P1, P2, and P3 were 75 μm , 110 and 95 μm , respectively. The P1-to-P2 and P2-to-P3 distances were 30 and 40 μm , respectively.

Film and Device Characterization

The crystallinities of perovskite films were characterized by a Shimadzu XRD-6100 diffractometer with Cu K α radiation. The UV–vis absorption spectra were recorded on an Agilent Cary 60 UV–vis spectrophotometer. The morphologies of the samples were characterized by SEM (JEOL JSM-7800F Prime). HRTEM samples were prepared by scraping the perovskite films from the glass substrate and collected on a TEM grid. ToF-SIMS analyses were carried out on a TOF-SIMS 5–100 (ION-TOF GmbH). The chemical states on the film surface were characterized by XPS (Kratos AXIS ULTRA HAS, monochromated Al K α = 1486.6 eV). The analysis of the XPS data was performed by using Casa XPS 2.3.16 software. GIWAXS measurements were performed at the BL14B1 line station of the Shanghai Synchrotron Radiation Facility (SSRF) with a beam wavelength of 0.1298 nm. PL and TRPL spectra were recorded at room temperature on a fluorescence spectrophotometer (FLS 1000). The TPV and TPC (Zahner PP211 and Zahner Zennium) measurements were generated by a microsecond pulse of white light incident on solar cells under open-circuit and short-circuit conditions, respectively. Current density–voltage (*J*–*V*) curves of perovskite solar cells were measured by a Keithley 2401 source meter under simulated AM 1.5G illumination (100 mW cm⁻²; Enlitech Class AAA Solar Simulator). EQE spectra were measured on an Enlitech QE-3011 system. The EQE-EL was measured by a Keithley 2400 source meter and a QE 65Pro spectrometer (Ocean Optics).

ASSOCIATED CONTENT

Supporting Information

The Supporting Information is available free of charge at <https://pubs.acs.org/doi/10.1021/jacsau.3c00469>.

Additional XRD; UV–vis absorption; XPS; ToF-SIMS; SEM; TPC; *J*–*V* characterization results; and certification report of the mini-modules (PDF)

AUTHOR INFORMATION

Corresponding Authors

Yixin Zhao – School of Environmental Science and Engineering, Frontiers Science Center for Transformative Molecules, Shanghai Jiao Tong University, Shanghai 200240, China; Shanghai Non-carbon Energy Conversion and Utilization Institute, Shanghai 200240, China; State Key Lab of Metal Matrix Composites, Shanghai Jiao Tong University, Shanghai 200240, China; orcid.org/0000-0002-8663-9993; Email: yixin.zhao@sjtu.edu.cn

Yuetian Chen – School of Environmental Science and Engineering, Frontiers Science Center for Transformative Molecules, Shanghai Jiao Tong University, Shanghai 200240,

China; Shanghai Non-carbon Energy Conversion and Utilization Institute, Shanghai 200240, China; orcid.org/0000-0003-3516-8199; Email: yuetian.chen@sjtu.edu.cn

Authors

Ning Wei – School of Environmental Science and Engineering, Frontiers Science Center for Transformative Molecules, Shanghai Jiao Tong University, Shanghai 200240, China

Yanfeng Miao – School of Environmental Science and Engineering, Frontiers Science Center for Transformative Molecules, Shanghai Jiao Tong University, Shanghai 200240, China

Xingtiao Wang – School of Environmental Science and Engineering, Frontiers Science Center for Transformative Molecules, Shanghai Jiao Tong University, Shanghai 200240, China

Zhixiao Qin – School of Environmental Science and Engineering, Frontiers Science Center for Transformative Molecules, Shanghai Jiao Tong University, Shanghai 200240, China

Xiaomin Liu – School of Environmental Science and Engineering, Frontiers Science Center for Transformative Molecules, Shanghai Jiao Tong University, Shanghai 200240, China

Haoran Chen – School of Environmental Science and Engineering, Frontiers Science Center for Transformative Molecules, Shanghai Jiao Tong University, Shanghai 200240, China

Haifei Wang – School of Environmental Science and Engineering, Frontiers Science Center for Transformative Molecules, Shanghai Jiao Tong University, Shanghai 200240, China

Yugang Liang – School of Environmental Science and Engineering, Frontiers Science Center for Transformative Molecules, Shanghai Jiao Tong University, Shanghai 200240, China

Shaowei Wang – School of Environmental Science and Engineering, Frontiers Science Center for Transformative Molecules, Shanghai Jiao Tong University, Shanghai 200240, China

Complete contact information is available at: <https://pubs.acs.org/10.1021/jacsau.3c00469>

Author Contributions

The manuscript was written through contributions of all authors with approvals given to the final version of the manuscript. CRediT: **Ning Wei** conceptualization, data curation, formal analysis, investigation, writing-original draft, writing-review & editing; **Yanfeng Miao** data curation, formal analysis, investigation, writing-review & editing; **Xingtiao Wang** data curation, formal analysis, investigation, writing-review & editing; **Zhixiao Qin** data curation, formal analysis, investigation, writing-review & editing; **Xiaomin Liu** data curation, formal analysis, investigation, validation, writing-review & editing; **Haoran Chen** data curation, formal analysis, investigation, writing-review & editing; **Haifei Wang** data curation, formal analysis, investigation; **Yugang Liang** data curation, formal analysis; **Shaowei Wang** data curation, formal analysis; **Yixin Zhao** conceptualization, formal analysis, funding acquisition, investigation, project administration, supervision, validation, writing-original draft, writing-review & editing; **Yuetian Chen** conceptualization, formal analysis,

funding acquisition, investigation, validation, writing-original draft, writing-review & editing.

Notes

The authors declare no competing financial interest.

ACKNOWLEDGMENTS

This work was supported by the National Natural Science Foundation of China (NSFC, Grant Nos. 22025505, 22220102002, and 22209111), Program of Shanghai Academic/Technology Research Leader (No. 20XD1422200), Natural Science Foundation of Shanghai (No. 23ZR1428000), and the Shanghai Pujiang Program (No. 22PJ1404700). The authors thank the Shanghai Synchrotron Radiation Facility for the assistance on GIWAXS measurements, and the Instrumental Analysis Centers in Shanghai Jiao Tong University and School of Environmental Science and Engineering for assistance with material characterization.

REFERENCES

- (1) NREL. Best Research-Cell Efficiency Chart. <https://www.nrel.gov/pv/assets/pdfs/best-research-cell-efficiencies.pdf> (accessed October 29, 2023).
- (2) Jena, A. K.; Kulkarni, A.; Miyasaka, T. Halide Perovskite Photovoltaics: Background, Status, and Future Prospects. *Chem. Rev.* **2019**, *119* (5), 3036–3103.
- (3) Kim, J. Y.; Lee, J.-W.; Jung, H. S.; Shin, H.; Park, N.-G. High-Efficiency Perovskite Solar Cells. *Chem. Rev.* **2020**, *120* (15), 7867–7918.
- (4) Schulz, P.; Cahen, D.; Kahn, A. Halide Perovskites: Is It All about the Interfaces? *Chem. Rev.* **2019**, *119* (5), 3349–3417.
- (5) Isikgor, F. H.; Zhumagali, S.; T Merino, L. V.; De Bastiani, M.; McCulloch, I.; De Wolf, S. Molecular Engineering of Contact Interfaces for High-Performance Perovskite Solar Cells. *Nat. Rev. Mater.* **2023**, *8* (2), 89–108.
- (6) Yang, Y.; Yang, M.; Moore, D. T.; Yan, Y.; Miller, E. M.; Zhu, K.; Beard, M. C. Top and Bottom Surfaces Limit Carrier Lifetime in Lead Iodide Perovskite Films. *Nat. Energy* **2017**, *2* (2), 16207.
- (7) Ni, Z.; Bao, C.; Liu, Y.; Jiang, Q.; Wu, W.-Q.; Chen, S.; Dai, X.; Chen, B.; Hartweg, B.; Yu, Z.; Holman, Z.; Huang, J. Resolving Spatial and Energetic Distributions of Trap States in Metal Halide Perovskite Solar Cells. *Science* **2020**, *367* (6484), 1352–1358.
- (8) Min, H.; Kim, M.; Lee, S.-U.; Kim, H.; Kim, G.; Choi, K.; Lee, J. H.; Seok, S. I. Efficient, Stable Solar Cells by Using Inherent Bandgap of α -Phase Formamidinium Lead Iodide. *Science* **2019**, *366* (6466), 749–753.
- (9) Lu, H.; Liu, Y.; Ahlwat, P.; Mishra, A.; Tress, W. R.; Eickemeyer, F. T.; Yang, Y.; Fu, F.; Wang, Z.; Avalos, C. E.; Carlsen, B. I.; Agarwalla, A.; Zhang, X.; Li, X.; Zhan, Y.; Zakeeruddin, S. M.; Emsley, L.; Rothlisberger, U.; Zheng, L.; Hagfeldt, A.; Grätzel, M. Vapor-Assisted Deposition of Highly Efficient, Stable Black-Phase FAPbI₃ Perovskite Solar Cells. *Science* **2020**, *370* (6512), eabb8985.
- (10) Hui, W.; Chao, L.; Lu, H.; Xia, F.; Wei, Q.; Su, Z.; Niu, T.; Tao, L.; Du, B.; Li, D.; Wang, Y.; Dong, H.; Zuo, S.; Li, B.; Shi, W.; Ran, X.; Li, P.; Zhang, H.; Wu, Z.; Ran, C.; Song, L.; Xing, G.; Gao, X.; Zhang, J.; Xia, Y.; Chen, Y.; Huang, W. Stabilizing Black-Phase Formamidinium Perovskite Formation at Room Temperature and High Humidity. *Science* **2021**, *371* (6536), 1359–1364.
- (11) Zhao, Y.; Ma, F.; Qu, Z.; Yu, S.; Shen, T.; Deng, H.-X.; Chu, X.; Peng, X.; Yuan, Y.; Zhang, X.; You, J. Inactive (PbI₂)₂RbCl Stabilizes Perovskite Films for Efficient Solar Cells. *Science* **2022**, *377* (6605), 531–534.
- (12) Park, J.; Kim, J.; Yun, H.-S.; Paik, M. J.; Noh, E.; Mun, H. J.; Kim, M. G.; Shin, T. J.; Seok, S. I. Controlled Growth of Perovskite Layers with Volatile Alkylammonium Chlorides. *Nature* **2023**, *616* (7958), 724–730.

- (13) Chen, T.; Foley, B. J.; Park, C.; Brown, C. M.; Harriger, L. W.; Lee, J.; Ruff, J.; Yoon, M.; Choi, J. J.; Lee, S.-H. Entropy-Driven Structural Transition and Kinetic Trapping in Formamidinium Lead Iodide Perovskite. *Sci. Adv.* **2016**, *2* (10), e1601650.
- (14) Nan, Z.-A.; Chen, L.; Liu, Q.; Wang, S.-H.; Chen, Z.-X.; Kang, S.-Y.; Ji, J.-B.; Tan, Y.-Y.; Hui, Y.; Yan, J.-W.; Xie, Z.-X.; Liang, W.-Z.; Mao, B.-W.; Tian, Z.-Q. Revealing Phase Evolution Mechanism for Stabilizing Formamidinium-Based Lead Halide Perovskites by a Key Intermediate Phase. *Chem* **2021**, *7* (9), 2513–2526.
- (15) Liu, X.; Luo, D.; Lu, Z.-H.; Yun, J. S.; Saliba, M.; Seok, S. I.; Zhang, W. Stabilization of Photoactive Phases for Perovskite Photovoltaics. *Nat. Rev. Chem.* **2023**, *7* (7), 462–479.
- (16) Degani, M.; An, Q.; Albaladejo-Siguan, M.; Hofstetter, Y. J.; Cho, C.; Paulus, F.; Grancini, G.; Vaynzof, Y. 23.7% Efficient Inverted Perovskite Solar Cells by Dual Interfacial Modification. *Sci. Adv.* **2021**, *7* (49), eabj7930.
- (17) Dai, Z.; Li, S.; Liu, X.; Chen, M.; Athanasiou, C. E.; Sheldon, B. W.; Gao, H.; Guo, P.; Padture, N. P. Dual-Interface-Reinforced Flexible Perovskite Solar Cells for Enhanced Performance and Mechanical Reliability. *Adv. Mater.* **2022**, *34* (47), 2205301.
- (18) Li, H.; Zhang, C.; Gong, C.; Zhang, D.; Zhang, H.; Zhuang, Q.; Yu, X.; Gong, S.; Chen, X.; Yang, J.; Li, X.; Li, R.; Li, J.; Zhou, J.; Yang, H.; Lin, Q.; Chu, J.; Grätzel, M.; Chen, J.; Zang, Z. 2D/3D Heterojunction Engineering at the Buried Interface towards High-Performance Inverted Methylammonium-Free Perovskite Solar Cells. *Nat. Energy* **2023**, *8*, 946.
- (19) Yang, D.; Zhou, X.; Yang, R.; Yang, Z.; Yu, W.; Wang, X.; Li, C.; Liu, S. Frank.; Chang, R. P. H. Surface Optimization to Eliminate Hysteresis for Record Efficiency Planar Perovskite Solar Cells. *Energy Environ. Sci.* **2016**, *9* (10), 3071–3078.
- (20) Yang, X.; Luo, D.; Xiang, Y.; Zhao, L.; Anaya, M.; Shen, Y.; Wu, J.; Yang, W.; Chiang, Y.; Tu, Y.; Su, R.; Hu, Q.; Yu, H.; Shao, G.; Huang, W.; Russell, T. P.; Gong, Q.; Stranks, S. D.; Zhang, W.; Zhu, R. Buried Interfaces in Halide Perovskite Photovoltaics. *Adv. Mater.* **2021**, *33* (7), 2006435.
- (21) Levine, I.; Al-Ashouri, A.; Musiienko, A.; Hempel, H.; Magomedov, A.; Drevilkauskaitė, A.; Getautis, V.; Menzel, D.; Hinrichs, K.; Unold, T.; Albrecht, S.; Dittrich, T. Charge Transfer Rates and Electron Trapping at Buried Interfaces of Perovskite Solar Cells. *Joule* **2021**, *5* (11), 2915–2933.
- (22) Qin, Z.; Chen, Y.; Wang, X.; Wei, N.; Liu, X.; Chen, H.; Miao, Y.; Zhao, Y. Zwitterion-Functionalized SnO₂ Substrate Induced Sequential Deposition of Black-Phase FAPbI₃ with Rearranged PbI₂ Residue. *Adv. Mater.* **2022**, *34* (32), 2203143.
- (23) Luo, C.; Zheng, G.; Gao, F.; Wang, X.; Zhan, C.; Gao, X.; Zhao, Q. Engineering the Buried Interface in Perovskite Solar Cells via Lattice-Matched Electron Transport Layer. *Nat. Photonics* **2023**, *17*, 856.
- (24) Fan, J.; Ma, Y.; Zhang, C.; Liu, C.; Li, W.; Schropp, R. E. I.; Mai, Y. Thermodynamically Self-Healing 1D-3D Hybrid Perovskite Solar Cells. *Adv. Energy Mater.* **2018**, *8* (16), 1703421.
- (25) Yang, N.; Zhu, C.; Chen, Y.; Zai, H.; Wang, C.; Wang, X.; Wang, H.; Ma, S.; Gao, Z.; Wang, X.; Hong, J.; Bai, Y.; Zhou, H.; Cui, B.-B.; Chen, Q. An *in Situ* Cross-Linked 1D/3D Perovskite Heterostructure Improves the Stability of Hybrid Perovskite Solar Cells for over 3000 h Operation. *Energy Environ. Sci.* **2020**, *13* (11), 4344–4352.
- (26) Zhan, Y.; Yang, F.; Chen, W.; Chen, H.; Shen, Y.; Li, Y.; Li, Y. Elastic Lattice and Excess Charge Carrier Manipulation in 1D–3D Perovskite Solar Cells for Exceptionally Long-Term Operational Stability. *Adv. Mater.* **2021**, *33* (48), 2105170.
- (27) Kong, T.; Xie, H.; Zhang, Y.; Song, J.; Li, Y.; Lim, E. L.; Hagfeldt, A.; Bi, D. Perovskite-Templated Formation of a 1D@3D Perovskite Structure toward Highly Efficient and Stable Perovskite Solar Cells. *Adv. Energy Mater.* **2021**, *11* (34), 2101018.
- (28) Xu, A. F.; Liu, N.; Xie, F.; Song, T.; Ma, Y.; Zhang, P.; Bai, Y.; Li, Y.; Chen, Q.; Xu, G. Promoting Thermodynamic and Kinetic Stabilities of FA-Based Perovskite by an *in Situ* Bilayer Structure. *Nano Lett.* **2020**, *20* (5), 3864–3871.
- (29) Liu, P.; Xian, Y.; Yuan, W.; Long, Y.; Liu, K.; Rahman, N. U.; Li, W.; Fan, J. Lattice-Matching Structurally-Stable 1D@3D Perovskites toward Highly Efficient and Stable Solar Cells. *Adv. Energy Mater.* **2020**, *10* (17), 1903654.
- (30) Miao, Y.; Wang, X.; Zhang, H.; Zhang, T.; Wei, N.; Liu, X.; Chen, Y.; Chen, J.; Zhao, Y. *In Situ* Growth of Ultra-Thin Perovskitoid Layer to Stabilize and Passivate MAPbI₃ for Efficient and Stable Photovoltaics. *eScience* **2021**, *1* (1), 91–97.
- (31) Chen, R.; Shen, H.; Chang, Q.; Tang, Z.; Nie, S.; Chen, B.; Ping, T.; Wu, B.; Yin, J.; Li, J.; Zheng, N. Conformal Imidazolium 1D Perovskite Capping Layer Stabilized 3D Perovskite Films for Efficient Solar Modules. *Adv. Sci.* **2022**, *9* (36), 2204017.
- (32) Jiao, H.; Ni, Z.; Shi, Z.; Fei, C.; Liu, Y.; Dai, X.; Huang, J. Perovskite Grain Wrapping by Converting Interfaces and Grain Boundaries into Robust and Water-Insoluble Low-Dimensional Perovskites. *Sci. Adv.* **2022**, *8* (48), eabq4524.
- (33) Tan, S.; Huang, T.; Yavuz, I.; Wang, R.; Yoon, T. W.; Xu, M.; Xing, Q.; Park, K.; Lee, D.-K.; Chen, C.-H.; Zheng, R.; Yoon, T.; Zhao, Y.; Wang, H.-C.; Meng, D.; Xue, J.; Song, Y. J.; Pan, X.; Park, N.-G.; Lee, J.-W.; Yang, Y. Stability-Limiting Heterointerfaces of Perovskite Photovoltaics. *Nature* **2022**, *605* (7909), 268–273.
- (34) Lee, J.-W.; Tan, S.; Seok, S. I.; Yang, Y.; Park, N.-G. Rethinking the A Cation in Halide Perovskites. *Science* **2022**, *375* (6583), eabj1186.
- (35) Zhang, H.; Miao, Y.; Gao, Y.; Zhao, Y.; Chen, J. Differentially Accelerated Electron and Hole Diffusion in MAPbI₃ Film Surface Treated by a Quaternary Ammonium Halide for High-Efficiency Solar Cells. *Energy Technol.* **2023**, *11* (1), 2200822.
- (36) Xue, J.; Wang, R.; Yang, Y. The Surface of Halide Perovskites from Nano to Bulk. *Nat. Rev. Mater.* **2020**, *5* (11), 809–827.
- (37) Lefler, B. M.; May, S. J.; Fafarman, A. T. Role of Fluoride and Fluorocarbons in Enhanced Stability and Performance of Halide Perovskites for Photovoltaics. *Phys. Rev. Mater.* **2020**, *4* (12), 120301.
- (38) Jang, C. H.; Harit, A. K.; Lee, S.; Kim, S. H.; Jeong, J.-E.; Park, J. H.; Jung, E. D.; Ha, J. M.; Kwak, S. K.; Woo, H. Y.; Song, M. H. Sky-Blue-Emissive Perovskite Light-Emitting Diodes: Crystal Growth and Interfacial Control Using Conjugated Polyelectrolytes as a Hole-Transporting Layer. *ACS Nano* **2020**, *14* (10), 13246–13255.
- (39) Bu, T.; Li, J.; Zheng, F.; Chen, W.; Wen, X.; Ku, Z.; Peng, Y.; Zhong, J.; Cheng, Y.-B.; Huang, F. Universal Passivation Strategy to Slot-Die Printed SnO₂ for Hysteresis-Free Efficient Flexible Perovskite Solar Module. *Nat. Commun.* **2018**, *9* (1), 4609.
- (40) Tress, W.; Yavari, M.; Domanski, K.; Yadav, P.; Niesen, B.; Correa Baena, J. P.; Hagfeldt, A.; Grätzel, M. Interpretation and Evolution of Open-Circuit Voltage, Recombination, Ideality Factor and Subgap Defect States during Reversible Light-Soaking and Irreversible Degradation of Perovskite Solar Cells. *Energy Environ. Sci.* **2018**, *11* (1), 151–165.
- (41) Cai, Y.; Cui, J.; Chen, M.; Zhang, M.; Han, Y.; Qian, F.; Zhao, H.; Yang, S.; Yang, Z.; Bian, H.; Wang, T.; Guo, K.; Cai, M.; Dai, S.; Liu, Z.; Liu, S. Frank. Multifunctional Enhancement for Highly Stable and Efficient Perovskite Solar Cells. *Adv. Funct. Mater.* **2021**, *31* (7), 2005776.
- (42) Dong, Q.; Fang, Y.; Shao, Y.; Mulligan, P.; Qiu, J.; Cao, L.; Huang, J. Electron-Hole Diffusion Lengths > 175 nm in Solution-Grown CH₃NH₃PbI₃ Single Crystals. *Science* **2015**, *347* (6225), 967–970.
- (43) Liu, Y.; Sun, J.; Yang, Z.; Yang, D.; Ren, X.; Xu, H.; Yang, Z.; Liu, S. F. 20-Mm-Large Single-Crystalline Formamidinium-Perovskite Wafer for Mass Production of Integrated Photodetectors. *Adv. Opt. Mater.* **2016**, *4* (11), 1829–1837.
- (44) Yao, J.; Kirchartz, T.; Vezie, M. S.; Faist, M. A.; Gong, W.; He, Z.; Wu, H.; Troughton, J.; Watson, T.; Bryant, D.; Nelson, J. Quantifying Losses in Open-Circuit Voltage in Solution-Processable Solar Cells. *Phys. Rev. Appl.* **2015**, *4* (1), 014020.